Electrokinetic flows in highly charged micro/nanochannel with Newtonian boundary slip condition

Myung-Suk Chun, Jang Ho Yun and Tae Ha Kim

Complex Fluids Lab., Korea Institute of Science and Technology (KIST)
Hawolgok-dong, Seongbuk-gu, Seoul 136-791, Republic of Korea, mschun@kist.re.kr

ABSTRACT

We have developed the explicit model incorporated together the finite difference scheme for electrokinetic flow in rectangular microchannels encompassing Navier's boundary slip. The externally applied body force originated from between the nonlinear Poisson-Boltzmann field around the channel wall and the flow-induced electric field is employed in the equation of motion. It is evident that the fluid slip counteracts the effect by the electric double layer (EDL) and induces a larger flow rate. Particle streak imaging by fluorescent microscope has been applied to microchannels designed to allow for flow visualization of dilute latex colloids underlying the condition of simple fluid. We recognized the behavior of fluid slip at the hydrophobic surface of polydimethylsiloxane (PDMS) wall, from which the slip length was evaluated for different conditions.

Keywords: electrokinetics, boundary slip, poisson-boltzmann, navier-stokes, nernst-planck, hydrophobic channel

1 INTRODUCTION

The physics of micro/nanofluids has become an area of intense interest both scientifically and technologically. The long-range nature of viscous flows and the small dimension inherent in confined spaces imply that the influence of boundaries is quite significant. Among the boundary effects, we should focus on the hydrodynamic slip at a solid-liquid interface and the electrokinetic phenomena [1-3]. The flow enhancement will benefit during the transport, since friction increases with the surface-to-volume ratio. We first provide the explicit model for rectangular microchannels with solvophobic smooth surfaces. Hydrophobic materials have become attractive for use in MEMS fabrications, and the surface of channel wall frequently has inhomogeneous properties. The slip length was obtained with the particle streak velocimetry using dilute colloids with variations of the shear rate and suspension pH.

2 BASIC CONSIDERATIONS

Many studies have contributed to the slip behavior in narrow channels, in which the Navier's fluid slip occurs in hydrophobic surfaces as depicted in Fig. 1. A slip length β inferred from measurements is the local equivalent distance below the solid surface at which the no-slip boundary condition would be satisfied if the flow field were extended linearly outside.

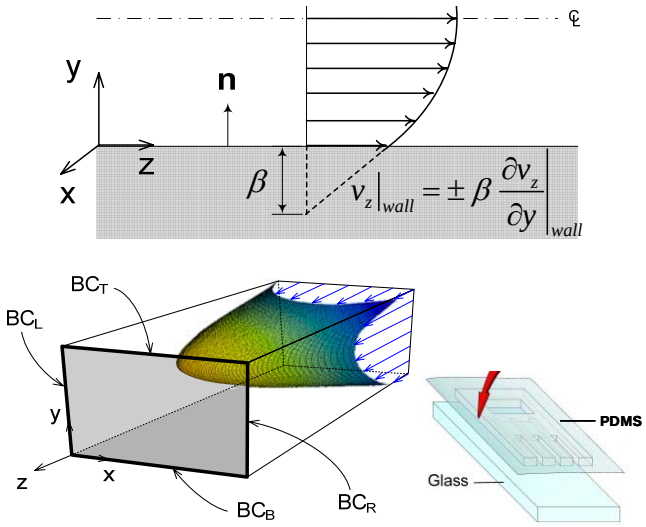

Figure 1: Fluid slip at hydrophobic surface (upper), and channel with different BCs (lower).

2.1 Electrokinetic Flow

For incompressible laminar flow, the velocity of ionic fluid is expressed as $\mathbf{v} = [0,0,v_z(x,y)]$, the pressure $p = p(z)$, and the flow-induced electric field $\mathbf{E} = [0,0,E_z(z)]$. Neglecting gravitational forces, the body force per unit volume ubiquitously caused by the z-directional action of flow-induced electric field E_z on the net charge density ρ_e can be written as $F_z = \rho_e E_z$ [4]. The E_z is defined by the flow-induced streaming potential ϕ as $E_z = -d\phi(z)/dz$. With these identities, the Navier-Stokes equation reduces to

$$\eta\left[\frac{\partial^2 v_z}{\partial x^2}+\frac{\partial^2 v_z}{\partial y^2}\right]=\frac{dp}{dz}-\rho_e E_z \quad . \tag{1}$$

Based on Eq. (1), the slip boundary condition at the hydrophobic surface is commonly expressed as $v_z|_{wall} = \pm\beta\left(\partial v_z/\partial y\right)\big|_{wall}$ in Fig. 1.

NSTI-Nanotech 2008, www.nsti.org, ISBN 978-1-4200-8505-1 Vol. 3

When the charged surface is in contact with an electrolyte, the electrostatic charge would influence the distribution of nearby ions. Consequently, an electric field is established and the positions of the individual ions in solution are replaced by the mean concentration of ions. For a rectangular channel, the nonlinear Poisson-Boltzmann (P-B) equation governing the electric potential field is given as [5]

$$\frac{\partial^2 \Psi}{\partial x^2} + \frac{\partial^2 \Psi}{\partial y^2} = \kappa^2 \sinh \Psi \quad . \tag{2}$$

Here, the dimensionless electric potential Ψ denotes $Ze\psi/kT$ and the inverse EDL thickness κ is defined by $\kappa = \sqrt{2n_b Z_i^2 e^2 / \varepsilon kT}$, where n_b is the electrolyte ionic concentration in the bulk solution at the electroneutral state, Z_i the valence of type *i* ions, e the elementary charge, ε the dielectric constant, and kT the Boltzmann thermal energy. The n_b ($1/m^3$) equals to the product of the Avogadro's number N_A (1/mol) and bulk electrolyte concentration (mM). The Boltzmann distribution of the ionic concentration of type *i* (i.e., $n_i = n_b \exp(-Z_i e\psi/kT)$) provides a local charge density $Z_i e n_i$. We determine the net charge density ρ_e ($\equiv \Sigma_i Z_i e n_i = Ze(n_+ - n_-)$), as follows

$$\rho_e = Zen_b \left[\exp(-\Psi) - \exp(\Psi)\right] = -2Zen_b \sinh \Psi \quad . \tag{3}$$

Substituting Eq. (3) into Eq. (1) yields

$$\frac{\partial^2 v_z}{\partial x^2} + \frac{\partial^2 v_z}{\partial y^2} = -\frac{1}{\eta}\frac{\Delta p}{L} + \frac{2Zen_b \sinh \Psi}{\eta}\frac{\Delta \phi}{L} \tag{4}$$

where L is channel length, $\Delta p = p_0 - p_L$, and $\Delta\phi = \phi_0 - \phi_L$.

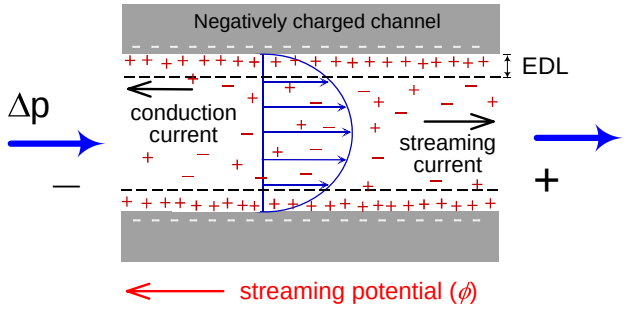

Figure 2: Electrokinetic streaming potential in channels.

In order to analyze the velocity profile, the net current conservation is applied in the microchannel taking into account the Nernst-Planck equation. This equation describes the transport of ions in terms of convection and migration resulting from the pressure difference and electric potential gradient, respectively. Ions in the mobile region of the EDL are transported through the channel, commonly causing the electric convection current (i.e., streaming current) I_S. The accumulation of ions provides the streaming potential difference $\Delta\phi$ (= $E_z L$). This field causes the conduction current I_C to flow back in the opposite direction. In this case, the net current I consists of I_S and I_C, and it should be zero at the steady state, viz. $I \equiv I_S + I_C = 0$ [6].

2.2 Finite Difference Scheme

Basic procedures of the present finite difference method are analogous to the previous work [4]. To obtain the solution of the nonlinear P-B equation with the boundary conditions imposed as $\Psi = \Psi_{s,L}$ at x = 0, $\Psi = \Psi_{s,R}$ at x = W, $\Psi = \Psi_{s,B}$ at y = 0, and $\Psi = \Psi_{s,T}$ at y = H, the five-point central difference method is taken on the left-hand side of Eq. (2). The sinh Ψ on the right-hand side can be linearized as $\sinh \Psi_{l,m}^k + \left(\Psi_{l,m}^{k+1} - \Psi_{l,m}^k\right)\cosh \Psi_{l,m}^k$, where *k* means the iteration index and the grid index *l* and *m* = 1, 2, … , N.

Illustrative computations are performed considering a fully developed flow of the aqueous electrolyte fluid in a 10 μm square microchannel with $\Delta p/L$ = 1.0 bar/m. The grids of 101×101 meshes were built within the channel and the convergence criterion is given to satisfy the accuracy requirement. The dielectric constant ε is given as a product of the dielectric permittivity of a vacuum and the relative permittivity for aqueous fluid. The fluid viscosity are taken as 1.0×10^{-3} kg/m·sec, at room temperature. For 1:1 type electrolyte, κ^{-1} (nm) is expressed as [*fluid ionic concentration* (M)]$^{-1/2}$/3.278. The EDL thicknesses correspond to 9.7, 96.5, and 965 nm for bulk electrolyte concentrations of 1.0, 10^{-2}, and 10^{-4} mM, where thinning of the EDL means the decrease of electrostatic repulsion.

As shown in Fig. 2, computations were performed with asymmetric variations of both slip length and long-range repulsion, because the hydrodynamic and electric properties depend on the material of the wall. The fluid slip induces a higher flow velocity, while the presence of EDL retards the flow rate. If the slip is absent, a higher apparent viscosity and a higher friction factor would be predicted.

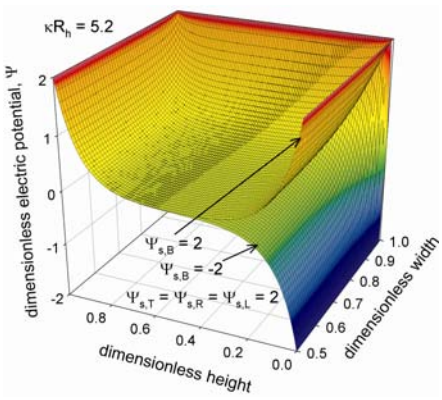

Figure 3: Simulation result of electric potential profile, where hydraulic radius R_h is 5μm.

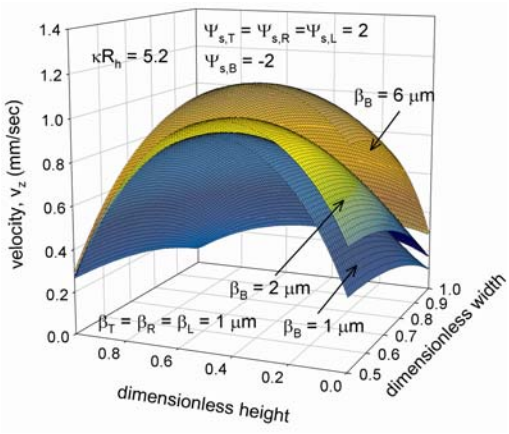

Figure 4: Simulation result of velocity profile, where hydraulic radius R_h is 5μm.

Further, we consider the electrokinetic flow in the serpentine channel that constitutes another source of the Taylor dispersion. The resultant velocity profiles are computed with variations of geometry curvature and electric surface potential.

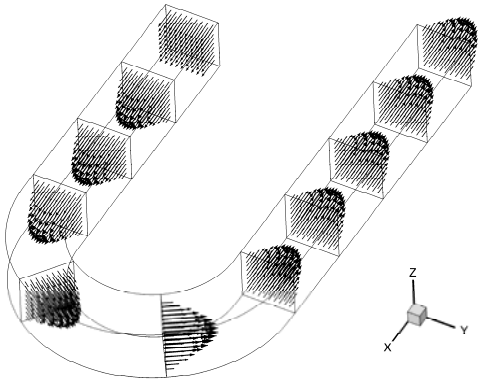

Figure. 5: Flow evolutions in curved rectangular channel.

3 FLOW VISUALIZATION EXPERIMENTS

Experimental observations provide benchmark data for the verification of theoretical study and developing novel micro processes [7]. Microfabrication procedures based on the MEMS micromachining are employed to prepare the microfluidic-chip using molded PDMS and glass cover. The velocity profile of dilute latex colloids was obtained in the channel of PDMS-glass as well as PDMS-PDMS chip shown in Fig. 6, by employing the inverted fluorescent microscope (Nikon, TE-2000) with particle streak velocimetry (PSV) on a parallel uniaxial flow field [8]. The motion of the bulk fluid in particle-based flow velocimetry is inferred from the observed velocity of marker particles. Seeding of the flow field was achieved with fluorescent polystyrene latex (Sigma L-5280, MO) of radius 1.05 μm and density of 1.003. A ratio of particle size to channel width is quite small, and the serpentine channel has also been considered besides the straight one.

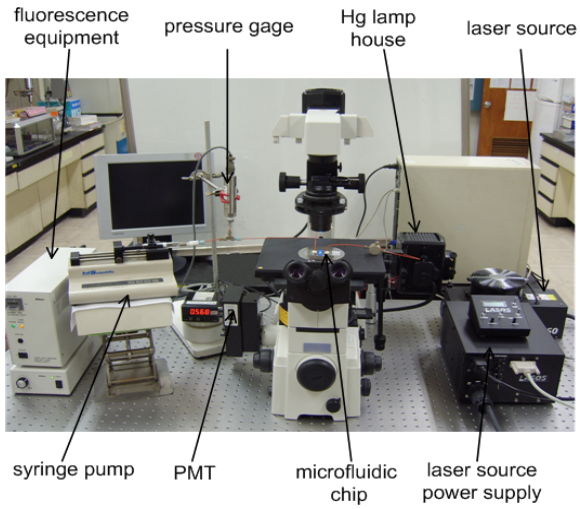

Figure 6: Experimental setup.

4 RESULTS

In Fig. 5, we observe the fluid slip at the hydrophobic surface of PDMS wall, which allows evaluation the value of slip length for different suspension conditions. The PDMS-PDMS channel resulted in a higher flow velocity than PDMS-glass one.

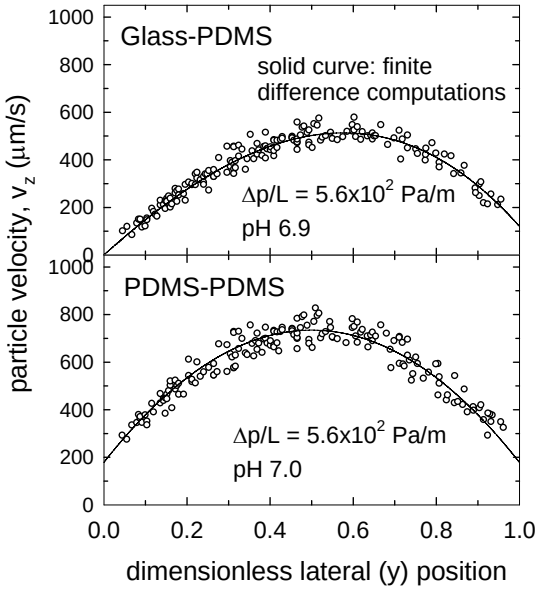

Figure 7: Uniaxial velocity profile in slit-like channel of glass-PDMS and PDMS-PDMS chip at 0.5 mM KCl electrolyte fluid.

NSTI-Nanotech 2008, www.nsti.org, ISBN 978-1-4200-8505-1 Vol. 3

The wettability increases by the introduction of surface charge, therefore, the slip length has a trend to decrease as the pH increases causing stronger electrokinetic effects, as shown in Fig. 8. When the fluid slip is absent, a higher friction factor would be predicted in view of the electroviscous effect. In Fig. 9, variations of slip length at PDMS wall are identified as around 1 μm for low shear rate (less than about 50 s^{-1}). We found that, as the nominal shear rate increases, the slip length increases but it appears to be independent of pH.

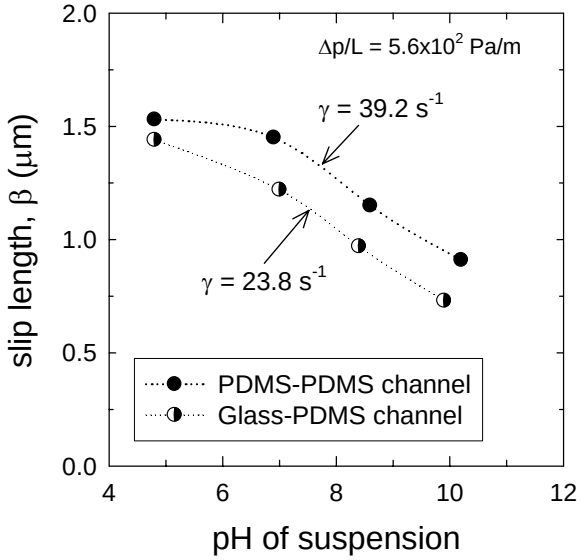

Figure 8: The variation of the slip length for different suspension pH.

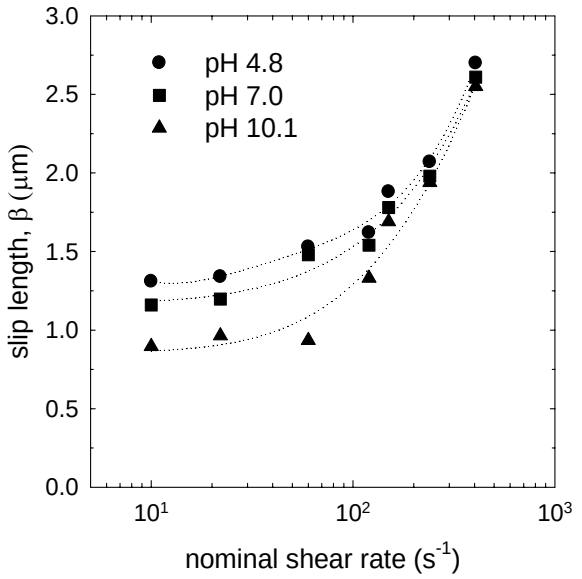

Figure 9: The variation of the slip length for PDMS-PDMS channels for different shear rate and suspension pH.

5 CONCLUSIONS

We developed the numerical scheme for electrokinetic flow with Navier's boundary slip in rectangular channels. The Stokes flow in confined spaces is influenced by the EDL, therefore, the fluid behavior in microchannels deviates from that described by the laminar flow equation in general. Newtonian fluid slip induces a larger flow velocity and then a lower friction factor would be predicted. The validity of the velocity profile determined by flow visualization was justified by comparing with the computational results, where a good agreement was found. Newtonian fluid slip at hydrophobic surfaces has been observed at the length scale of several micrometers, and it is available to obtain the dependency of slip length on the shear rate and suspension pH.

ACKNOWLEDGEMENTS

This work was supported by the KOSEF (R01-2004-000-10944-0) as well as the KIST (μTAS Research: 2E19690).

REFERENCES

[1] D.C. Tretheway and C.D. Meinhart, Phys. Fluids 14, L9, 2002.
[2] E. Lauga and H.A. Stone, J. Fluid Mech. 489, 55, 2003.
[3] P. Joseph, C. Cottin-Bizonne, J.-M. Benoit, C. Ybert, C. Journet, P. Tabeling and L. Bocquet, Phys. Rev. Lett. 97, 156104, 2006.
[4] M.-S. Chun, T.S. Lee and N.W. Choi, J. Micromech. Microeng. 15, 710, 2005.
[5] R.F. Probstein, "Physicochemical Hydrodynamics: An Introduction", Wiley, 185-198, 1994,
[6] C. Werner, H. Körber, R. Zimmermann, S. Dukhin and H.-J. Jacobasch, J. Colloid Interface Sci. 208, 329,1998.
[7] M.-S. Chun, M.S. Shim, N.W. Choi, Lab Chip 6, 302, 2006.
[8] M.H. Oddy, J.G. Santiago and J.C. Mikkelsen, Anal. Chem. 73, 5822, 2001.